# A Novel Hybrid Suspension Electromagnet for Middle-low Speed Maglev Train

## Han Weitao[1], Sun Jinji[2]*, Liu Xiankai[1], Guo Haixia[1], and Wang Jinsha[1]

[1]*CRRC Qingdao Sifang CO., LTD, Qingdao 266111, China*
[2]*School of Instrumentation Science & Opto-electronics Engineering, Science and Technology on Inertial Laboratory,
Beihang University, Beijing 100191, China*

This paper proposes a novel hybrid suspension electromagnet for application in the middle-low speed maglev train. Its configuration and working principle are introduced. Mathematical models of the suspension force and guidance force are established accurately by equivalent magnetic circuit method (EMCM), from which the relationships of suspension force-control current-suspension gap and guidance force-guidance displacement are derived. Finite element method (FEM) is also applied to analyze the performances and characteristics of the novel hybrid suspension electromagnet. The analysis results are in good agreement with those calculated by EMCM, which is helpful in designing and optimizing the suspension system. The comparisons are made between the performances of the novel and the traditional electromagnets. The contrast results indicate that the proposed hybrid suspension electromagnet possesses better performances compared to the traditional structure, especially the little control current and the low suspension power loss.

## 1. Introduction

As a new type of transportation, maglev trains play an important role in the development of the track traffic, which own extraordinary features due to absence of friction, such as safety, low-noise and environmentally friendly compared to the traditional railways [1-4]. The middle-low speed maglev train is suspended by the attractive magnetic force from the traditional electromagnets, which is normally composed of U-type iron core and control coil, as shown in Fig. 1.

When the control coil is stimulated with electricity, the electromagnetic field and suspension force are produced between the F-type track and the U-type iron core [5-7]. However, the suspension power loss is huge because the magnetic field is provided absolutely by the control coil stimulated with a high current. The high power loss is a serious problem to middle-low speed maglev train, which will result in a high temperature rise of the electromagnets and make the sensors extremely hot. This bad condition may affect the reliability and security of the

suspension system seriously [8-9]. So it's necessary to reduce the suspension power loss for the commercial application of middle-low speed maglev train.

To solve the power loss problem, researchers studied the hybrid suspension electromagnet by introducing a permanent magnet to the traditional electromagnet and various types of structures are proposed, reducing the power loss remarkably [10-12]. The permanent magnet can provide the biased magnetic field, so the magnetic fluxes generated by the control current can be reduced
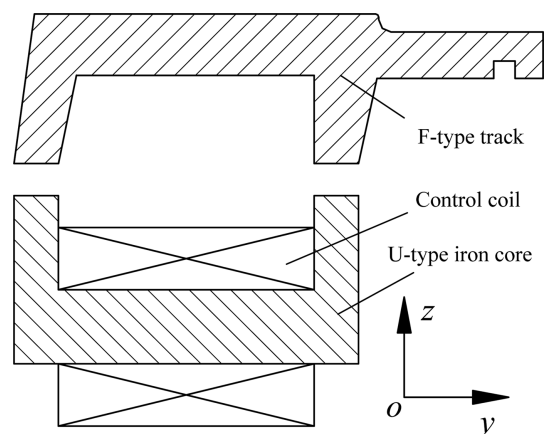


**Fig. 1.** Structure sketch map of traditional electromagnet.

*Corresponding author: Tel: +86-10-8233-9273
Fax: +86-10-8231-6813, e-mail: sunjinji2001@163.com

with the constant suspension resultant force. And then, the control current and the power loss will decrease. In [13-14], hybrid suspension electromagnets are proposed whose permanent magnets are located on the top surfaces of iron core roles. It's convenient to adjust the thickness of the permanent magnets for the carrying capacity, but the permanent magnets are damaged easily when the electromagnets strike on the F-type track in an emergency. In [15], the permanent magnet is embedded in the center of the U-type iron core, which avoids the issue of damage effectively. The permanent magnet has an identical section area with the U-type iron core in this scheme, which is improved further by enlarging the section area in [16-18]. As a result, the reluctance of the permanent magnet decreases and the carrying capacity is enhanced. Whereas, the electromagnetic fluxes still pass through the permanent magnet, so the adjustment ability of the control coil is weakened as the magnetic potential loss in the permanent magnet. In addition, the load of the whole coach is not taken into consideration in the performance analysis of the electromagnet.

Considering the suspension power loss and the adjustment ability of the control coil, a novel hybrid suspension electromagnet is designed through introducing a permanent magnet into the U-type iron core as well as a non-ferromagnetic block that can reduce the electromagnetic potential loss.

## 2. Structure and Working Principle

### 2.1. Structure

The configuration of the novel electromagnet is shown in Fig. 2, which consists of U-type iron core, permanent magnet, non-ferromagnetic block and control coil. Suspension gaps exist between the F-type track and the U-type iron core. Considering structure strength and magnetic saturation simultaneously, steel is selected as the
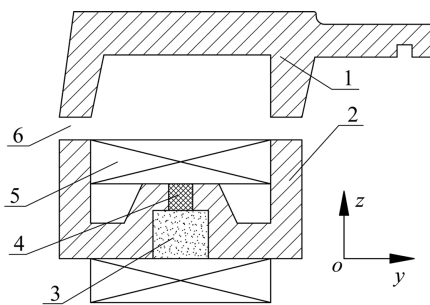
material of the F-type track and the U-type iron core. The permanent magnet magnetized in the y direction is made of the rare earth material featuring higher coercive force and lower temperature factor. The non-ferromagnetic block made of aluminum alloy will be regarded as an air gap in the magnetic field analysis equivalently, which can make the electromagnetic fluxes avoid passing through the permanent magnet and decrease the magnetic potential loss effectively. The control coil made of aluminum foil operates with the permanent magnet together to realize the stabile suspension of maglev train.

### 2.2. Working principle

The magnetic flux paths of the novel electromagnet are schematically shown in Fig. 3. In the ideal state, maglev train maintains equilibrium with an appropriate suspension gap under the action of the suspension force. At this moment, the suspension force is equal to the gravity of maglev train and the control current remains stable. However, the electromagnet will be disturbed continuously during the practical operating process of maglev train.

While the electromagnet is disturbed and produces a displacement $\Delta z$ in the $+z$ direction, the flux densities of the suspension gaps increase, leading to the suspension force increasing greater than the gravity, so the resultant force will make the electromagnet move along the $+z$ direction further. Then the displacement sensors detect the motion and transmit a signal to the control system which will reduce the control current to weaken the flux densities of the suspension gaps. As a result, the suspension force decreases and the resultant force drives the electromagnet to the equilibrium position. In the same way, while the electromagnet produces a displacement $\Delta z$ in the $-z$ direction, the resultant force will make it far away from the F-type track. The control system will raise the control current to increase the suspension force accord-
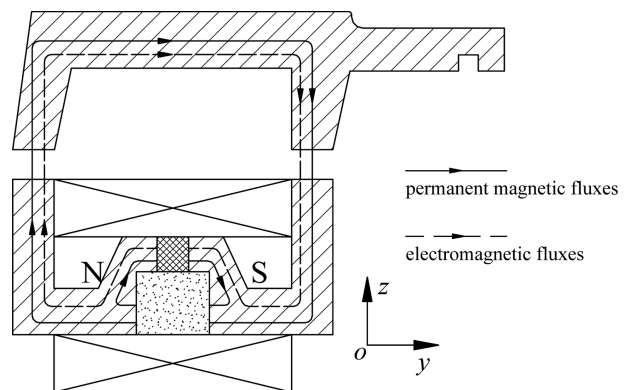


1-F-type track, 2-U-type iron core, 3-Permanent magnet, 4-Non-ferromagnetic block, 5-Control coil, 6-Suspension gap

**Fig. 2.** Structure sketch map of the novel hybrid suspension electromagnet.



**Fig. 3.** Flux paths of the novel hybrid suspension electromagnet.

ingly, thus maintaining the appropriate suspension gaps.

While the electromagnet is disturbed in the $y$ direction, the suspension gaps will be distorted because the poles of the F-type track and the electromagnet own an identical width. Due to the distorted suspension gaps, leakage fluxes are produced and provide a passive guidance force, which makes maglev train possess the capability of guidance.

## 3. Analysis of Performance

### 3.1. Mathematic model of suspension force

There are four parallel electromagnets in an electromagnet module applied in the middle-low speed maglev train. To simplify the calculation, one electromagnet is selected as the analytic object. In addition, the reluctances of the magnetic material are ignored and the leakage fluxes are approximated by a leakage coefficient. The parameters of the electromagnet model are displayed in Fig. 4, on which the corresponding equivalent magnetic circuits are built based and shown in Fig. 5 and Fig. 6. $F_{pm}$ is the magnetic motive force of the permanent magnet. $NI$ is the magnetic motive force of the control coil, wherein $N$ and $I$ are the number of turns and the current of the control coil respectively. $R_{pm}$ and $R_2$ are the reluctances of the permanent magnet and the non-ferromagnetic block respectively. $R_{11}$ and $R_{12}$ are the reluctances of
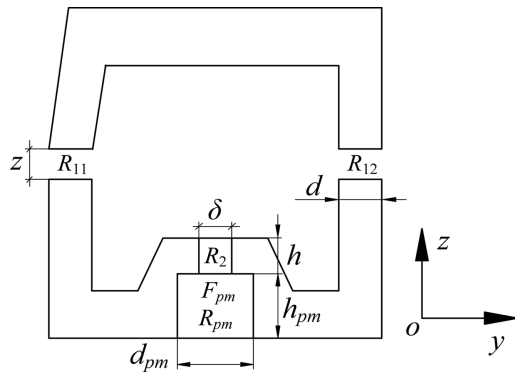


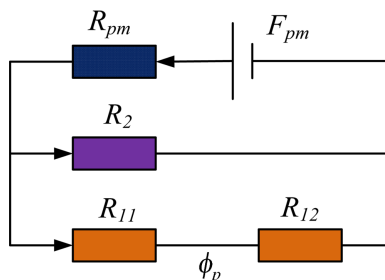**Fig. 4.** Reluctances display with suspension gap $z$.



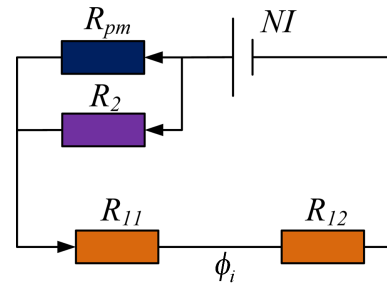**Fig. 5.** (Color online) Equivalent magnetic circuit of permanent magnetic fluxes.



**Fig. 6.** (Color online) Equivalent magnetic circuit of electromagnetic fluxes.

the suspension gaps. $\phi_p$ and $\phi_i$ are the permanent magnetic fluxes and the electromagnetic fluxes in the suspension gaps respectively.

Based on Fig. 5 and Fig. 6, $\phi_p$ and $\phi_i$ can be calculated as

$$\phi_p = \frac{F_{pm}R_m}{\sigma(R_{pm}+R_m)(R_{11}+R_{12})} \tag{1}$$

$$\phi_i = \frac{NI}{R_{11}+R_{12}+R_i} \tag{2}$$

Where $\sigma$ denotes the leakage flux coefficient of the permanent magnet; $R_m$ and $R_i$ are given by

$$R_m = (R_{11}+R_{12})//R_2 \tag{3}$$

$$R_i = R_{pm}//R_2 \tag{4}$$

The reluctances can be calculated as

$$\begin{cases} R_{11} = R_{12} = \dfrac{z}{u_0 A_1} \\[2mm] R_2 = \dfrac{\delta}{u_0 A_2} \\[2mm] R_{pm} = \dfrac{d_{pm}}{u_0 A_m} \end{cases} \tag{5}$$

Where $z$ and $A_1$ denote the height and the area of the suspension gaps; $\delta$ and $A_2$ denote the width and the area of the non-ferromagnetic block; $d_{pm}$ and $A_m$ denote the width and the area of the permanent magnet; $u_0$ is the permeability of vacuum.

By the principle of virtual work, the suspension force is expressed as [19]

$$F_z = \frac{(\phi_P + \phi_i)^2}{u_0 A_1} \tag{6}$$

Substituting (1) through (5) into (6), the suspension force can be obtained.

### 3.2. Mathematic model of guidance force
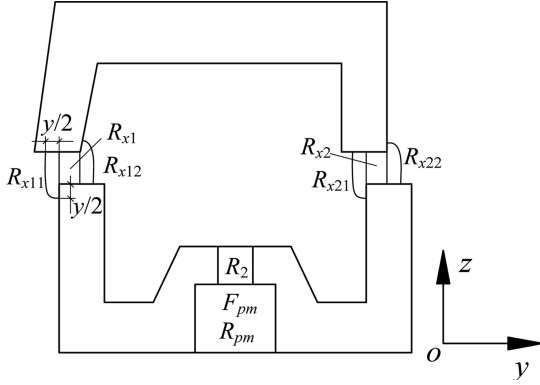
When the middle-low speed maglev train travels on the

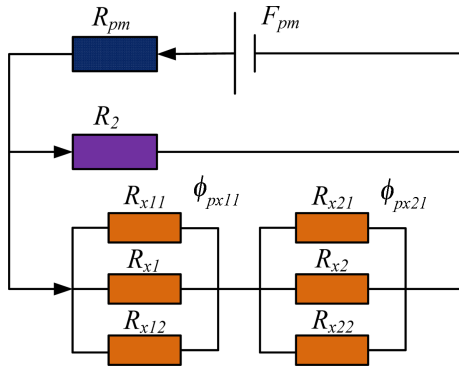**Fig. 7.** Reluctances display with guidance displacement $y$.



**Fig. 8.** (Color online) Equivalent magnetic circuit of permanent magnetic fluxes.



**Fig. 9.** (Color online) Equivalent magnetic circuit of electromagnetic fluxes.

curve passage of the F-type track, the electromagnet will drive off the F-type track in the y direction. As a passive resilience, the guidance force can introduce maglev train to pass through the curve passage stably. Whereas the guidance force generated by the leakage fluxes is un-controllable, so it's important to analyze it and ensure the reliable guidance capability.

Figure 7 shows the reluctances displayed in the electro-magnet model, when the electromagnet translates a dis-placement $y$ in the +y direction. The corresponding equi-valent magnetic circuits built are shown in Fig. 8 and Fig. 9.

$R_{x11}$, $R_{x1}$, $R_{x12}$, $R_{x21}$, $R_{x2}$ and $R_{x22}$ are the reluctances of the suspension gaps. $\phi_{px11}$ and $\phi_{px21}$ are the permanent magnetic fluxes of the reluctances $R_{x11}$ and $R_{x21}$ respec-tively. $\phi_{ix11}$ and $\phi_{ix21}$ are the electromagnetic fluxes of the reluctances $R_{x11}$ and $R_{x21}$ respectively.

Based on Fig. 8, $\phi_{px11}$ and $\phi_{px21}$ can be calculated as

$$
\begin{cases}
\phi_{px11} = \dfrac{F_{pm}R_{xm}R_{xm1}}{\sigma(R_{pm}+R_{xm})(R_{xm1}+R_{xm2})R_{x11}} \\[2ex]
\phi_{px21} = \dfrac{F_{pm}R_{xm}R_{xm2}}{\sigma(R_{pm}+R_{xm})(R_{xm1}+R_{xm2})R_{x21}}
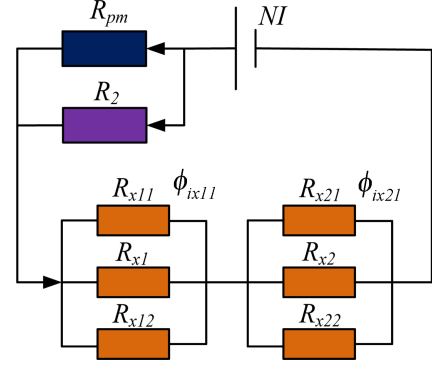\end{cases} \tag{7}
$$

Based on Fig. 8, $\phi_{ix11}$ and $\phi_{ix21}$ can be calculated as

$$
\begin{cases}
\phi_{ix11} = \dfrac{NIR_{xm1}}{(R_i+R_{xm1}+R_{xm2})R_{x11}} \\[2ex]
\phi_{ix21} = \dfrac{NIR_{xm2}}{(R_i+R_{xm1}+R_{xm2})R_{x21}}
\end{cases} \tag{8}
$$

Where $R_{xm}$, $R_{xm1}$ and $R_{xm2}$ are given by

$$
\begin{cases}
R_{xm} = R_2 //(R_{xm1}+R_{xm2}) \\
R_{xm1} = R_{x11}//R_{x1}//R_{x12} \\
R_{xm2} = R_{x21}//R_{x2}//R_{x22}
\end{cases} \tag{9}
$$

The reluctances of the suspension gaps can be express-ed as

$$
R_{x11} = R_{x12} = R_{x21} = R_{x22} = \frac{z}{u_0 A_x} \tag{10}
$$

Where $A_x$ denotes the area of the rectangle whose width is $y/2$ and length in the $x$ direction is $l$.

According to [20-21], the leakage fluxes of the suspension gaps increase with the guidance displacement $y$ increasing, then the reluctance $R_{x1}$ and $R_{x2}$ can be expressed as

$$
R_{x1} = R_{x2} = 1/(\frac{1}{R}+\frac{\lambda(y)}{R}) \tag{11}
$$

Where $R = z/(u_0 A)$ and $\lambda(y) = \alpha y/d$; $\lambda(y)$ is the correc-tion coefficient and $\alpha$ is a constant related to the structure of the electromagnet; $A = (d-y)l$ and $d$ denotes the width of the electromagnet poles.

Then, the guidance force is given by

$$
F_y = \frac{(\phi_{px11}+\phi_{ix11})^2}{2u_0 A_x} + \frac{(\phi_{px21}+\phi_{ix21})^2}{2u_0 A_x} = \frac{(\phi_{px11}+\phi_{ix11})^2}{u_0 A_x} \tag{12}
$$

Substituting (7) through (11) into (12), the guidance

**Table 1.** Parameters of the novel electromagnet.

| | |
|---|---|
| Height of permanent magnet, $h_{pm}$/mm | 65 |
| Width of permanent magnet, $d_{pm}$/mm | 60 |
| Height of magnetic isolation block, $\delta$/mm | 15 |
| Width of magnetic isolation block, $h$/mm | 20 |
| Width of electromagnet poles, $d$/mm | 28 |
| Length of electromagnet, $l$/mm | 0.42 |
| Coercive force of permanent magnet, $H_{pm}$/(kA/m) | 796 |
| Leakage coefficient of flux, $\sigma$(Suspension force) | 1.52 |
| Leakage coefficient of flux, $\sigma$(Guidance force) | 1.21 |
| Turn of control coil, $N$/turn | 360 |
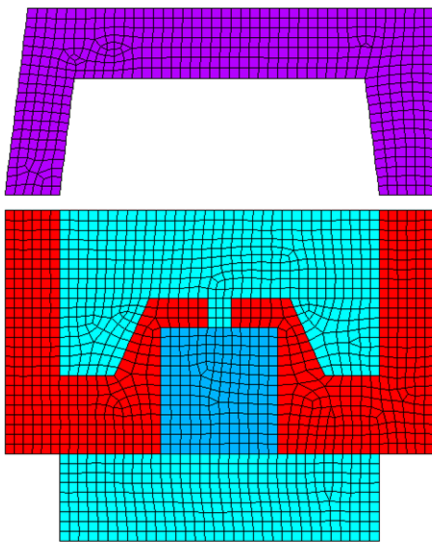


**Fig. 10.** (Color online) 2D FEM model of novel electromagnet.



(a) $F_z$-$z$ characteristic



(b) $B$-$z$ characteristic

**Fig. 11.** (Color online) Characteristics of novel electromagnet ($i = 0$).

force can be obtained. Then the guidance displacement stiffness can be derived by
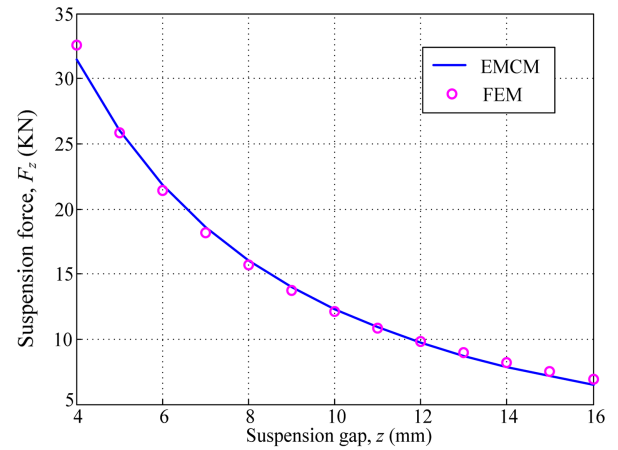
$$K_y = \frac{dF_y}{dy} \tag{13}$$
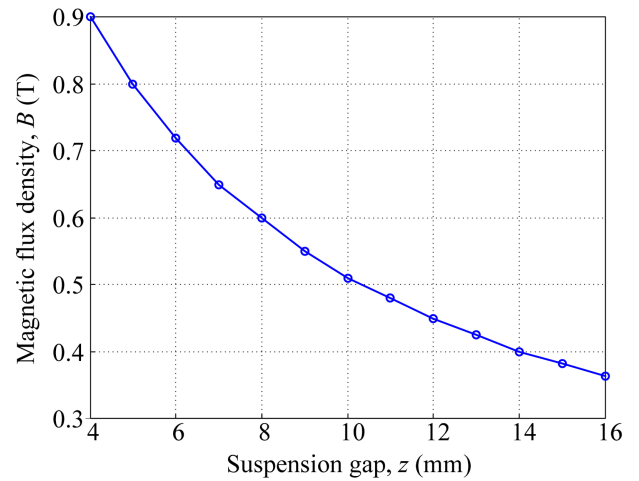
### 3.3. FEM model and analysis

FEM is widely applied in the electromagnetic calculation and design because of its high precision. Therefore, the mathematical model of the novel electromagnet can be validated by FEM. The main parameters of the novel electromagnet are shown in Table 1. Considering computation efficiency, a 2-D finite element model is established and shown in Fig. 10. This element model adopts the PLANE53 element and the nonlinear materials define by B-H curves.

3.3.1. Suspension force

As the Fig. 11(a) and Fig. 12(a) show, the characteri-

stics of the suspension force calculated by EMCM and FEM are consistent. In Fig. 11, the suspension force is totally provided by the permanent magnetic fluxes with the control current $i = 0$, which will decrease with decrease in the suspension gap. Generally the appropriate suspension gap $z$ for the middle-low speed maglev train is 8 mm at the ideal state of suspension, when the permanent magnetic force is 15.7 kN and the permanent magnetic flux density of the suspension gaps is 0.6T according to Fig. 11(b).

The suspension force will increase with increase in the control current in Fig. 12(a). There are all 10 electromagnet modules contained in one coach whose load are 32t based on the design requirement, so the suspension force of one electromagnet modules should reach 32 kN to counterbalance the gravity. The control current at the stable state of suspension calculated by the formula (6) is 18.3A and the magnetic flux density is 0.85T at the
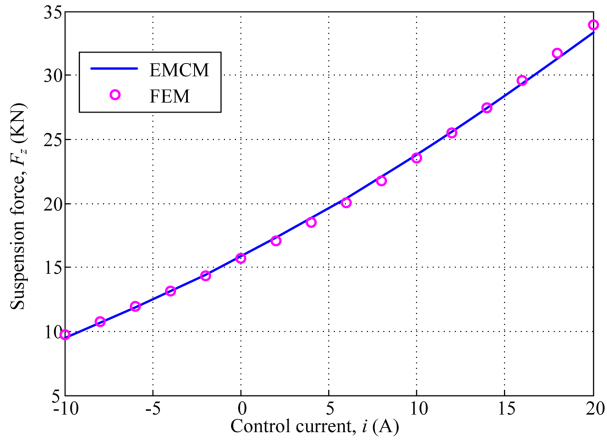
(a) $F_z$-$i$ characteristic
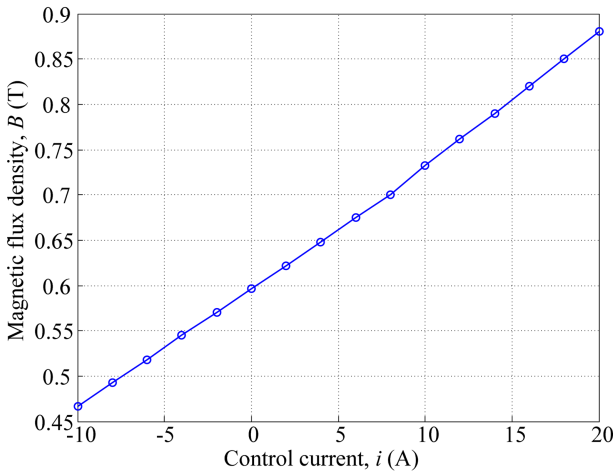


(b) $B$-$i$ characteristic

**Fig. 12.** (Color online) Characteristics of novel electromagnet ($z = 8$ mm).



**Fig. 13.** (Color online) $F_z$-$i$-$z$ characteristic within large variation range.
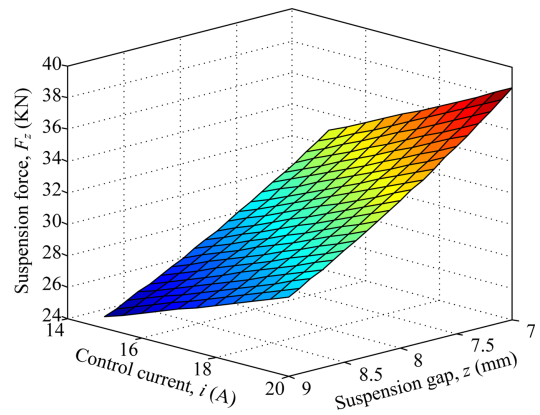


**Fig. 14.** (Color online) $F_z$-$i$-$z$ characteristic within small variation range.

moment according to Fig. 12(b). The permanent magnetic flux density is 0.6T based on the analysis before, and then the electromagnetic one is 0.25T, predicating the permanent magnetic fluxes lead a dominant role in the suspension force. If the suspension gap increases under a certain disturbance, the control current will become greater than 18.3A. On the contrary, the control current will become smaller than 18.3A even reverse and increase.

The characteristic of suspension force-control current-suspension gap presented in Fig. 13 is a curve surface, illustrating it's nonlinear within a larger variation range of the suspension gap and control current. However, at the static suspension state, the suspension gap and control current vary slightly with $z$ maintaining near 8mm and $i$ near 18.3A. When 16A < $i$ < 20A and 7 mm < $z$ < 9 mm, the characteristic of suspension force-control current-suspension gap is approximate a plane shown in Fig. 14, which demonstrates that suspension force-control current
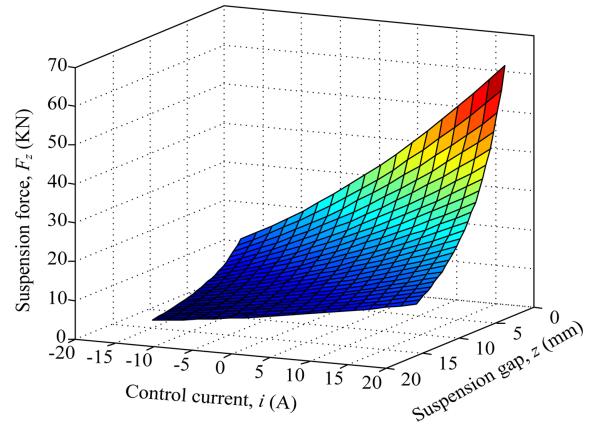
and suspension force-suspension gap possess good linear relationships. Linearizing the formula (6) and the linearized equation can be derived

$$F_z \approx \frac{\partial F_z}{\partial z}\Big|_{\substack{z=8 \\ i=18.8}} (z-8) + \frac{\partial F_z}{\partial i}\Big|_{\substack{z=8 \\ i=18.8}} (i-18.3) + 32000 \quad (14)$$

The first and second coefficients of the equation (14) can be called suspension displacement stiffness $K_x$ and current stiffness $K_i$ respectively. Through calculation, $K_x = 460$ N/mm and $K_i = 1000$ N/A. Then the suspension force at the static suspension state can be simplified as

$$F_z = 460z + 1000i + 9520 \quad (15)$$

The simplified linearizing equation (15) can benefit the control system. While maglev train operates at a high speed, the variation ranges of the suspension gap and the control current may expand widely. Therefore, the non-linear characteristic of suspension force-control current-suspension gap need to be considered in the control system.
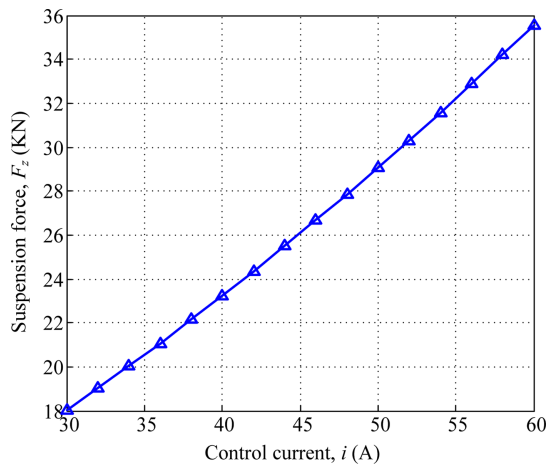
**Fig. 15.** (Color online) $F_z$-$i$ characteristic of novel electromagnet ($z = 16$ mm).



**Fig. 17.** (Color online) $K_y$-$y$ characteristic of novel electromagnet ($z = 8$ mm and $i = 18.3$A).

At the startup state, maglev train falls on the track and the suspension gap $z$ is 16 mm. The permanent magnetic force is very little and just 6.7 kN without the control current shown in Fig. 11(a). Then the control system raises the control current continually until reach 32 kN. The startup current calculated based on Fig. 15 is 54.9A. The permanent magnetic flux and electromagnetic flux densities are 0.36T and 0.49T respectively, when it's the electromagnetic fluxes that lead a dominant role in the suspension force.

### 3.3.2. Guidance force

Figure 16 presents the characteristics of guidance force-guidance displacement at the stable suspension state. Analysis results illustrate that the guidance force-gui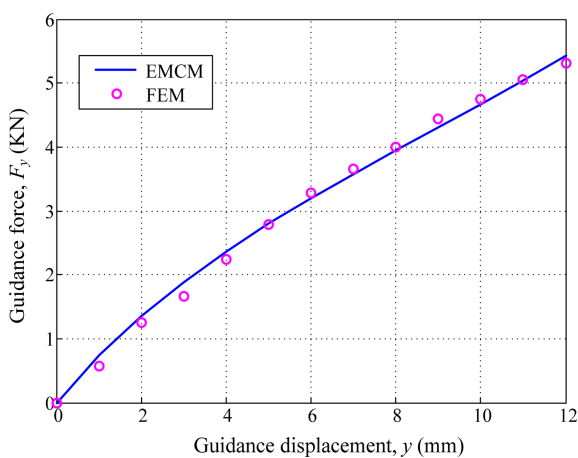dance displacement relationship derived by EMCM are in good agreement with the one by FEM. The guidance force increases with increase in the guidance displacement, so when the middle-low speed maglev train travels through the curve passage of the F-type track, the guidance displacement will enlarge continually until that the guidance force can counteract the disturbance force. However, the guidance displacement stiffness $K_y$ decreases simultaneously as illustrated in Fig. 17. A higher guidance displacement stiffness is beneficial to guarantee the suspension stability, because the guidance force is uncontrollable. Therefore, the middle-low speed maglev train should decelerate and pass through the curve passage at a lower speed. For example, if the guidance displacement $y = 6$ mm, the guidance force is 3.3 kN and the guidance displacement stiffness is 96.8 kN/mm based on formula (12) and (13).



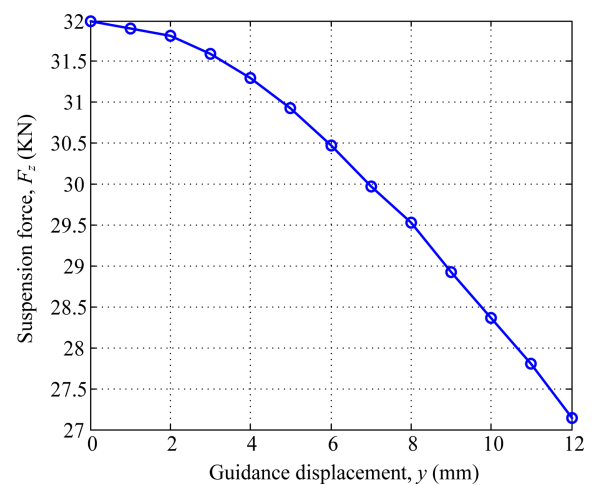**Fig. 16.** (Color online) $F_y$-$y$ characteristic of novel electromagnet ($z = 8$ mm and $i = 18.3$A).
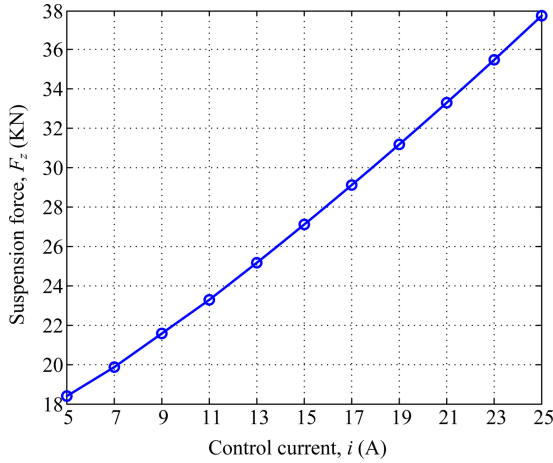


**Fig. 18.** (Color online) $F_z$-$y$ characteristic of novel electromagnet ($z = 8$ mm and $i = 18.3$A).

**Fig. 19.** (Color online) $F_z$-$i$ characteristic of novel electromagnet ($z = 8$ mm and $y = 6$ mm).



**Fig. 20.** (Color online) $F_z$-$i$ characteristics of traditional electromagnet.

### 3.4. Coupling analysis of the suspension force and guidance force

As aforementioned, the guidance force is generated by the distorted suspension gaps due to a displacement in the y direction, which will make the valid areas of suspension gaps decrease, and then influence the suspension force. In a word, if only the guidance force emerges, the suspension force will be affected in a way. The characteristic of suspension force-guidance displacement is given in Fig. 18. When the guidance displacement is small, the suspension force decreases slowly, but it becomes obvious as the guidance displacement increases further. Consequently, the control current should be raised actively to avoid the maglev train falling on the curve passage. In Fig. 18, the guidance displacement $y = 6$ mm and the suspension force is about 30.5 kN, which is not enough to suspend the maglev train. So the control current is raised to 19.3A based on Fig. 19.

## 4. Contrast between the Novel and Traditional Electromagnets

In this section, some performances of the novel and traditional electromagnets are compared. The precondition of the contrast analysis is that the key parameters are identical, such as turns of control coil, widths of electromagnet roles. Moreover, the volumes of these two types of electromagnets are as identical as possible. Similar to the novel electromagnet, a 2-D finite element model of the traditional one is established and the analysis results are shown in Fig. 20 and Table 2.

Analysis results demonstrate that the startup currents for these two types of electromagnets are nearly identical, which of the novel electromagnet is just smaller by 2.7A.
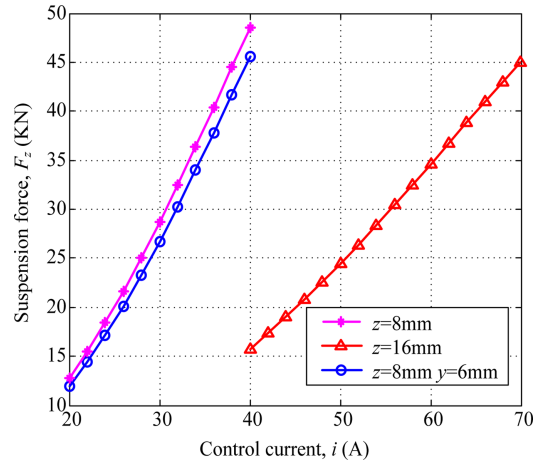
**Table 2.** Performances contrast of two types of electromagnets.

| Performance | Novel | Traditional |
|---|---|---|
| Startup current/A | 54.9 | 57.6 |
| Suspension current/A | 18.3 | 31.8 |
| Suspension current increase/A ($y = 6$ mm) | 1 | 1.2 |

However, the suspension currents of two types of electromagnets differ markedly, which of the novel electromagnet is much smaller than the traditional one (is decreased by 42.5%). It means that the suspension power loss and heat will reduce substantially, which is a great advantage for the maglev train. In addition, the suspension currents of the novel and traditional electromagnets will be all raised slightly on the curve passage similarly.

## 5. Conclusion

In this paper, a novel hybrid suspension electromagnet applied in the middle-low speed maglev train is proposed, whose performances are analyzed in details. Analysis results indicate that the suspension and guidance forces can satisfy the operating requirement preferably. Moreover, the suspension current of the novel electromagnet decreases obviously compared to the traditional one as a permanent magnet is introduced to the U-type iron core, which solves the main issue of the high power loss and heat for the maglev train effectively. The adjustment ability of the control coil is also enhanced by applying a non-ferromagnetic block to avoid the electromagnetic fluxes through the permanent magnet. The novel hybrid suspension electromagnet possessing excellent performances can improve the operating condition, so it's more appropriate for the middle-low speed maglev train.

## Acknowledgement

## References

[1] M. Morishita, T. Azukizawa, S. Kanda, N. Tamura, and T. Yokoyama, IEEE Trans. Vehi. Tech. **38**, 230 (1989).

[2] H. W. Lee, K. C. Kim, and J. Lee, IEEE Trans. Magn. **42**, 1917 (2006).

[3] G. Bohn, and G. Steinmetz, Int. Conf. MAGLEV Transport '85, 107 (1985).

[4] M. G. Pollard, and E. E. Riches, Int. Conf. MAGLEV Transport '85, 123 (1985).

[5] L. Shaoke, N. Hongyan, and Z. Kuikui, Urban Mass Transit, **10**, 22 (2007).

[6] M. Takahashi, G. Kwok, and K. Kubota, Proc. Maglev. **1**, 1 (2006).

[7] L. Shaoke, N. Hongyan, and Z. Kuikui, Electr. Drive Locomotives **2**, 36 (2007).

[8] Y. Yoshihide, F. Masaaki, T. Masao, and I. Syunzo, Proc. Maglev. 76 (2004).

[9] G. Roger, Proc. Maglev. 926 (2004).

[10] Y. K. Tzeng and T. C. Wang, IEEE Trans. Magn. **30**, 4731 (1994).

[11] L. Shaoke, G. Zhongjun, and C. Guirong, ICECE, 5 (2010).

[12] L. I. Yun-Gang, Y. Z. Yan, and C. Hu, J. National University of Defense Tech. **28**, 94 (2006) (in Chinese).

[13] S. H. Xu, Z. G. Xu, N. Q. Jin, and L. M. Shi, Proc. 18th Int. Conf. Maglev Syst. Linear Drivers, 26 (2004).

[14] Z. G. Xu, N. Q. Jin, L. M. Shi, and S. H. Xu, Proc. Maglev. Proc. 1019 (2004).

[15] L. Wang, J. Xiong, K. L. Zhang, and J. S. Lian, J. China Railw. Soc. **27**, 50 (2005) (in Chinese).

[16] Z. Zhang, L. She, L. Zhang, C. Shang, and W. Chang, IET Elec. Syst. in Trans. **1**, 61 (2011).

[17] F. Safaei, A. A. Suratgar, A. Afshar, and M. Mirsalim, IEEE Trans. Ener. Conv. **30**, 1163 (2015).

[18] S. K. Liu, B. An, S. K. Liu, and Z. J. Guo, IET Elec. Power Appl. **9**, 223 (2015).

[19] J. C. Fang, J. Sun, and H. Fan, Magnetically Suspended Inertial Momentum Wheel Technology, National Defense Industry Press, Beijing (2012) pp.120-125.

[20] J. J. Sun, Z. Y. Jun, W. T. Han, and G. Liu, J. Magn. Magn. Mater. **421**, 86 (2017).

[21] E. Y. Hou and K. Liu, IEEE Trans. Magn. **48**, 38 (2012).